

Anisotropic and Inhomogeneous Eddy-Induced Transport in Flows with Jets

IGOR KAMENKOVICH, PAVEL BERLOFF AND IRINA I. RYPINA

28.1 Introduction

In this chapter, we discuss material transport in a flow with eddies and jets, and how interactions between these flow components affect the distribution of various properties in oceans and atmospheres. We adopt a broad definition of eddies as geostrophic deviations from the mean flows, and assume that the time and/or length scales of eddies and the mean flow are very different. Note that this definition includes waves, coherent vortices, meanders, large-scale transients, non-stationary jets and other similar forms of flow variability, but excludes non-geostrophic currents and waves. Eddies play a key role in the distribution of such dynamically and climatically important quantities as potential vorticity and heat, as well as salt and biogeochemical tracers in the oceans, and moisture, aerosols and various trace gasses in the atmosphere. Among many examples of the importance of oceanic eddies are the maintenance of the stratification in the Antarctic Circumpolar Current (ACC) (e.g., Marshall and Radko, 2003; Meredith and Hogg, 2006) and of the Northern Hemisphere thermocline (e.g., Cessi and Fantini, 2004; Henning and Vallis, 2004), and control of the penetration of transient atmospheric gases into the North Atlantic (Booth and Kamenkovich, 2008). In the atmosphere, the importance of the mid-latitude eddy-induced transport in the meridional temperature structure has been long recognized (e.g., Lorenz, 1967); and eddy mixing is widely believed to play a key role in tracer distribution (Hunt and Manabe, 1968; Clark and Rogers, 1978, among many).

This chapter focuses on anisotropic and inhomogeneous properties of the eddy-induced transport, that is, its dependence on direction and geographical location, and explores the link between these properties and jets. The magnitude of the eddy-induced transport in most of the World Ocean is comparable to that of the mean advection, and a large part of the discussion of transport anisotropy is devoted to the oceans. The oceanic eddy length scale is also very small in comparison to the size of the oceanic basins, and the eddy-induced transport often has to be parameterized in numerical simulations, which adds practical importance to studies of the eddy-induced mixing. In contrast, powerful mean atmospheric advection homogenizes tracers in the along-stream direction, and research has traditionally concentrated on the cross-stream mixing and largely ignored the along-stream transport. We begin this chapter with the discussion of eddy diffusivity (section 28.2) and evidence for anisotropic mixing in the atmospheres and oceans (section 28.3). The mechanisms causing anisotropic transport in the presence of nearly stationary jets, most common in the

Earth and planetary atmospheres, are discussed in section 28.5. The importance of zonally elongated, jet-like transients for anisotropic transport is considered separately in section 28.6; these transients are particularly important in the parts of the ocean where the stationary jets tend to be weak relative to the eddies (so-called “latent jets”). Additional effects of nondiffusive dispersion of tracers, which can be linked to the jets’ dynamics, and ocean-specific importance of the large-scale potential vorticity (PV) distributions and topography are discussed last in section 28.7.

28.2 Eddy diffusivity

The efficiency of eddies in downgradient isopycnal tracer transport has been conventionally quantified by turbulent (“eddy”) diffusion, under an assumed analogy between the turbulent transport and molecular diffusion. As discussed below, this analogy is not straightforward in realistic geophysical flows, but the convenience of the eddy diffusion model is hard to argue against. Under the assumptions of homogeneous and isotropic turbulence, the diffusivity K can be related to the rms Lagrangian velocity $\langle vt \rangle$ of fluid particles and the Lagrangian decorrelation length scale l_{corr} or time scale τ_{corr} (e.g. Vallis, 2006):

$$K \sim \langle vt \rangle l_{corr} \sim \langle vt \rangle^2 \tau_{corr} \quad (28.1)$$

In the Eulerian analog of the above equation, the $\langle vt \rangle^2$ becomes the eddy kinetic energy (EKE), l_{corr} – the Eulerian mixing length, and τ_{corr} – the Eulerian time scale. These quantities were first introduced by Taylor (1921a) and Prandtl (1925) and remain a popular framework for the studies of eddy mixing. The Eulerian version of (28.1) is particularly convenient, since the eddy kinetic energy and length/time scales can be estimated from altimetry data directly, without deployment of Lagrangian drifters or relying on numerical simulations. Earlier studies of eddy diffusivities in the oceans focused on relations between the eddy kinetic energy and diffusivities (Keffer and Holloway, 1988b; Stammer, 1998), and there is a correlation between these two quantities if the length scale is taken to be the Rossby deformation radius (Sallee et al., 2008). The derivation of a universal relationship between the eddy diffusivity, energy and the length/time scales is, however, challenging, since the variables that would enter such a relationship may depend on depth and geographical location (Lumpkin et al., 2002;

Griesel et al., 2010) and also vary in time. This complexity is in large part explained by the effects of the mean flow and eddy propagation which cause significant deviations of l_{corr} from lengthscales of eddies (Klockner and Abernathey, 2014, section 28.5). The relationship between the Eulerian and Lagrangian time/length scales also depends on the flow regime. For example, in rapidly changing eddy fields, the Lagrangian lengthscale is much shorter than the Eulerian one, whereas the time scales are similar (Middleton, 1985), because particles travel a short distance before the eddy field changes. In contrast, the lengthscales are similar, and the Lagrangian time scale is much shorter than the Eulerian, if particles sample many eddies before the eddy field can change.

The eddy diffusivity, K , can be estimated in observational data and numerical simulations by either Lagrangian or Eulerian techniques. The former approach is based on trajectories of Lagrangian drifters or floats (e.g., Owens, 1984; Davis, 1991; LaCasce, 2008a). In the theoretical limit of an infinite number of these floats, their dispersion becomes equivalent to the evolution of tracer concentration. We will use the Lagrangian framework in most of this chapter because of its convenience for discussing two-dimensional and non-diffusive properties of the material transport and its direct relevance to real Lagrangian observation.

A practical method of estimating diffusivity is based on calculating the dispersion of an ensemble of Lagrangian particles relative to its center of mass (e.g. LaCasce, 2008a). The diffusivity is a tensor, and the discussion in this chapter is limited to lateral diffusivity (horizontal or isopycnal), so this tensor is two-dimensional. The diffusivity components in the x - and y -directions can be determined by (Kamenkovich et al., 2009a)

$$K_x(t) = \frac{1}{2} \frac{\partial D_x}{\partial t}, \quad K_y(t) = \frac{1}{2} \frac{\partial D_y}{\partial t} \quad (28.2)$$

where the dispersion in each direction D_x and D_y , are defined as

$$D_x(t) = \frac{1}{N} \sum_{n=1}^N \left(x_n(t) - \frac{1}{N} \sum_{n=1}^N x_n(t) \right)^2, \quad (28.3)$$

$$D_y(t) = \frac{1}{N} \sum_{n=1}^N \left(y_n(t) - \frac{1}{N} \sum_{n=1}^N y_n(t) \right)^2$$

and x_n and y_n are the zonal and meridional displacements of an n -th particle from its initial position. In the purely diffusive regime, typically achieved after several τ_{corr} , the dispersion is a linear function of time and diffusivities in (28.2) are constants. The deviations from this regime can, however, be substantial and will be discussed in section 28.7.1.

A tracer-based Eulerian approach that involves calculation of tracer contour deformation (Nakamura, 1996b) can only characterize cross mean-flow component of diffusivity, and is not suitable for this particular study. Similarly, estimates of the irreversible mixing from the tracer variance budget (Osborn and Cox, 1972; Abernathey and Marshall, 2013) provide the diffusivity only along the mean tracer gradient. Two-dimensional diffusivity tensor can also be estimated from direct estimates of non-rotational (divergent) eddy fluxes or their divergence (e.g.

Abernathey et al., 2013), although a consistent correlation between these fluxes and large-scale property gradients is generally challenging to establish (e.g. Gille and Davis, 1999; Nakamura and Chao, 2000; Roberts and Marshall, 2000; Solovov et al., 2002). An extension of this technique is based on multiple synthetic tracers that are oriented in zonal and meridional directions and advected by the eddying flow (Fox-Kemper et al., 2013; Bachman et al., 2015). A least-square method is then used to estimate a diffusivity tensor from assuming a linear relationship between eddy fluxes and large-scale gradients of these tracers and minimizing the remaining mismatch (“tracer scatter”).

The concept of eddy diffusivity has significant practical importance for ocean modeling. In particular, the majority of numerical ocean models lack the spatial resolution needed for explicit simulation of eddies, and, therefore, the effects of eddies have to be parameterized. The vast majority of these parameterizations are based on downgradient diffusion, with diffusivity parameters determined empirically and often taken to be spatially homogeneous and isotropic. These assumptions, despite being practically convenient, can lead to missing physics. The issue of eddy parameterization is less relevant to atmospheric modeling, since modern climate models are capable of resolving the Rossby deformation radius in the atmosphere.

28.3 Evidence for anisotropic eddy-induced transport

Evidence based on observational estimates, numerical simulations, and lab experiments suggests that the eddy-induced transport is not spatially homogeneous and isotropic and that some of these properties can be associated with mean flows. Studies of tracer transport in the Earth’s stratosphere clearly indicate suppressed cross-jet exchange at the cores of the strong and eastward polar night jets and weaker and westward subtropical jets that appear in summer (Allen and Nakamura, 2001b; Haynes and Shuckburgh, 2000a,b; Shepherd, 2007; Beron-Vera et al., 2008a). In the upper troposphere and lower stratosphere, the meridional mixing intensity also exhibits significant longitudinal variations within the subtropical jets, with well-pronounced mixing minima in local winter and where the jet is strongest (d’Ovidio et al., 2009; Shuckburgh et al., 2009a, Fig.28.1). These sharp minima in the eddy diffusivity indicate transport barriers and strong mixing regions (“surf zones”) to the north and south of jet core, and this structure strongly affects meridional distribution of atmospheric gases and aerosols. The most famous example of these effects is the barrier in the stratospheric boundary of the Antarctic Vortex (e.g. Juckes and McIntyre, 1987; Joseph and Legras, 2002; Rypina et al., 2007a; Beron-Vera et al., 2010) that facilitates the formation of the ozone hole in local spring.

The most striking feature of the atmosphere of Jupiter is a sequence of alternating stripes of different color, belts and zones, with different chemical composition; see chapter 4. Wind speed measurements made by Cassini spacecraft in 2000 suggest that the associated atmospheric circulation consists of a sequence of alternating prograde and retrograde jets (Porco and Co-authors, 2003; Vasavada and Showman, 2005), and that most boundaries between adjacent belts and zones coincide with the jet cores.

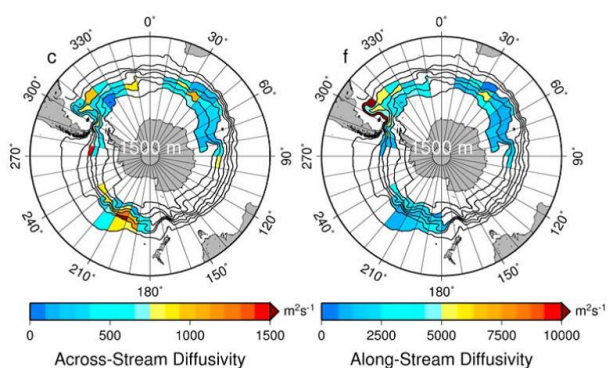


Figure 28.2 Evidence for inhomogeneous and anisotropic eddy transport. Cross-stream and along-stream diffusivities ($m^2 s^{-1}$); note the different color scale) in the numerical simulations of Lagrangian trajectories (deployment depth of 1500m) at $1/10^\circ$ spatial resolution; the effects of the mean advection are corrected for. Adapted from Griesel et al. (2010). ©John Wiley and Sons, Inc. Used with permission.

Dec 2000-Feb 2001

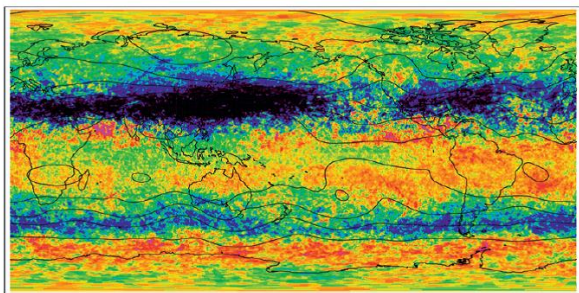


Figure 28.1 Estimates of the cross-stream eddy diffusivity in the atmosphere at the 350K level, using Lyapunov exponents during the period of Dec. 2000–Jan 2001. Note the presence of mixing zones and barriers, indicated by local minima (blue colors). Adapted from d’Ovidio et al. (2009). ©American Meteorological Society. Used with permission.

Assuming that the chemicals within belts and zones are not continuously produced in these regions, this feature implies very little meridional exchange between neighboring belts and zones and strongly suggests the existence of transport barriers at the cores of both prograde and retrograde jets. The barriers indeed exist at the axes of alternating jets in numerical models (Greenslade and Haynes, 2008; Beron-Vera et al., 2008a) and in laboratory experiments (Sommeria et al., 1989b; Read et al., 2007a). At the same time, the spread of debris after an impact of Comet SL9 fragments upon Jupiter appears to be inconsistent with the presence of such barriers (Galperin et al., 2014a, also see chapter 29). The efficiency of the transport barriers in the Jupiter’s atmosphere needs to be estimated as new data become available.

In the oceans, the mean circulation includes nearly zonal currents of the ACC, large-scale gyre circulation and various jets. Two types of jets are discussed in this chapter: strong western boundary currents, such as the Gulf Stream and Kuroshio, and multiple nearly zonal jets. After flowing next to the coast,

western boundary currents extend into the oceanic interior as strong meandering jets and are clearly seen in all observational datasets. Multiple jets are observed within the ACC and within the midlatitude gyres, and are often hidden behind the powerful eddy field (or “latent”; see complete discussion of ocean jets in chapter 3). Both types of jets have significant influence on the eddy-induced transport. For example, the eddy diffusivities in the North Atlantic and Pacific are very different between the western part of the basin, which is dominated by the Gulf Stream and Kuroshio, and the more quiescent eastern part (e.g. Holloway, 1986b; LaCasce and Bower, 2000a; Nakamura and Chao, 2000; Rypina et al., 2012). This can be partly explained by higher eddy kinetic energy (equation 28.1) in the vicinity of the western boundary currents observed in real data and numerical simulation and consistent with the inherent instability of these currents.

Eddy-induced oceanic transport is typically anisotropic, that is, it has a well-defined direction of maximum transport. Global analysis of the diffusivity tensor from surface drifters and tracer-based estimates from model simulations show several regions where the diffusivity tensor is anisotropic (Fox-Kemper et al., 2013). This anisotropy is most pronounced in regions with strong mean advection, such as ACC and the adjacent regions, western boundary regions and tropics. In the ACC, eddy diffusivities and Lagrangian statistics exhibit a significant difference between the along- and cross-stream directions, with the along-stream Lagrangian time/length scales being longer, as shown by the analysis of surface drifters (Sallee et al., 2008, with $K_x/K_y \approx 3$) and comprehensive numerical simulations (Griesel et al., 2010, with $K_x/K_y \approx 5$; Fig.28.2). ACC is the only predominantly zonal and circumpolar oceanic current, and the analogy to the subtropical atmospheric jets is tempting. As in the atmosphere, the meridional mixing in ACC can be suppressed, which can partly explain the anisotropy (Ferrari and Nikurashin, 2010b); see also discussion in Section 2.5.3 in this book. North of the ACC, where the mean gyre circulation is weak and inherently two-dimensional, the persistent anisotropy in the eddy-induced transport is intriguing and remains poorly understood. Bauer et al. (2002) analysed drifting buoys in the tropical Pacific and demonstrated substantial differences in the zonal and meridional diffusivities ($K_x/K_y \approx 7$). In the North Atlantic, various estimates provided further evidence for the anisotropy, including: (i) Freeland et al. (1975); (ii) Spall et al. (1993b) analysis of the subsurface floats in the Mediterranean outflow that produced $K_x/K_y \approx 2.5$; (iii) O’Dwyer et al. (2000) analysis of neutrally buoyant floats – Fig.28.3; (iv) McClean et al. (2002) analysis of surface drifters and a high-resolution state-of-the-art GCM; (v) Kamenkovich et al. (2009a) analysis of Lagrangian particles in a GCM – $K_x/K_y \approx 3 - 20$ (depending on depth).

Recent advances in quantifying anisotropy and inhomogeneity of the eddy-induced transport were made by Rypina et al. (2012), who analysed trajectories of both synthetic Lagrangian particles (diagnosed from altimetric data) and the actual surface drifters in the North Atlantic. In this study, the coordinate $x - y$ frame in 28.3–28.2 was rotated locally to achieve a maximal ratio between K_x and K_y and to diagonalise the diffusivity tensor. The study also applied an effective technique of calculat-

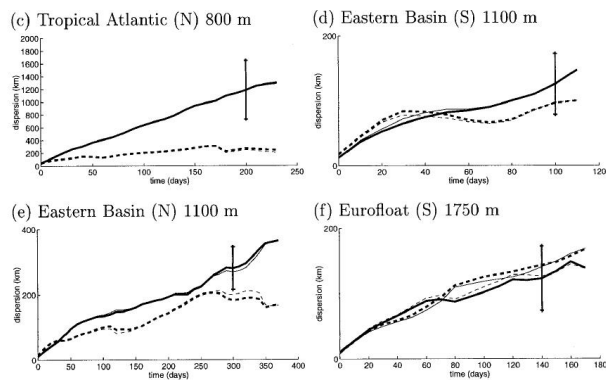


Figure 28.3 Evidence for inhomogeneous and anisotropic eddy transport. Eddy dispersion of neutrally buoyant floats in the real North Atlantic, evaluated along and across the mean PV contours (thick lines, respectively, solid and dashed), and in zonal and meridional directions (thin lines, respectively, solid and dashed). Adapted from (O'Dwyer et al., 2000). ©American Meteorological Society. Used with permission.

ing eddy-induced diffusivities in the presence of the mean flow (see also Berloff and McWilliams, 2002) – the “full-trajectory following” (FTF) method. This method accounts for the modulations of the eddy-induced dispersion by the mean-flow advection, that carries particles across the spatially varying eddy field. The FTF method thus places particles along Lagrangian trajectories in the full flow (eddies and mean), but calculates the particle dispersion due to eddies only. The method was shown to capture the known effects of mean advection, such as transport barriers in a meandering jet (Rypina et al., 2012).

These results consistently demonstrate that the direction of the maximum transport is not always zonal (Fig.28.4) and does not align with mean PV contours, and that the transport anisotropy is caused by geostrophic, rather than non-geostrophic currents (see also Sallee et al., 2008). The comparison of diffusivity estimates obtained with and without the kinematic mean-flow effects demonstrates the importance of these effects in the vicinity of the Gulf Stream (Fig.28.4), with the enhanced along-stream diffusivity, but nearly unchanged cross-stream one. The anisotropy, however, remains significant even if mean-flow effects are removed. The latter result strongly suggests that the jets can modulate the anisotropy (see also sections 28.5.2–28.5.4), but these effects cannot fully explain anisotropic properties (see also section 28.6).

28.4 Significance of anisotropy

While the overall importance of spatial inhomogeneity in eddy diffusivity (such as the presence of transport barriers) for tracer distribution can be easily anticipated, the significance of anisotropy in the diffusivity tensor is in some cases less straightforward. The preferential direction of the eddy transport is in many cases aligned with the direction of the mean current, especially if the mean current is sufficiently strong (at least comparable in magnitude to eddy velocities) and parallel (spatial variations in the along-stream directions are much weaker than in the trans-

verse direction). An example of such mean flow is an atmospheric or an oceanic jet, and in this case it is convenient to describe the transport anisotropy in terms of the along-stream and cross-stream diffusivities. The along-stream diffusivity can be dwarfed by very strong mean advection, such as that in the atmospheric jetstreams and in parts of the ACC. In these situations, only the cross-flow diffusivity is significant, and the discussion in this chapter relevant to the Earth and planetary atmospheres will be focused on modulations of this quantity (such as transport barriers).

The two-dimensional structure of the diffusivity tensor (both along- and cross-stream diffusivities) is important in most of the oceans, especially away from ACC and such strong boundary currents as the Gulf Stream or Kuroshio. In particular, assume that the mean advection dominates evolution of a tracer anomaly if $U/L \gg K/L^2$, where U , K and L are the scales for the mean advection, eddy diffusivity and size of the tracer anomalies, respectively. A strong oceanic current of more than $0.1 m sec^{-1}$, characteristic for the boundary currents and some parts of the ACC, will indeed dominate the tracer distribution if the along-stream diffusivity is less than $10,000 m^2 sec^{-1}$, and L is longer than 1000 km. The along-stream diffusivity, however, should be important for the rest of the World Ocean.

Approximating an anisotropic diffusivity tensor by a scalar diffusivity can lead to misleading results. In the case $K_x \gg K_y$, such an estimate would result in overestimated mixing in the y -direction and underestimated mixing in the x -direction. Furthermore, the estimate can produce unphysical *negative* diffusivity if the original tensor is not diagonal (Fox-Kemper et al., 2013).

The importance of eddy-induced transport and its anisotropy for tracer distribution in the ocean interior was further illustrated by Kamenkovich et al. (2015) who analysed the anisotropic diffusivity tensor estimated (using the FTF method) from numerical simulations of the QG “double-gyre” flow – an idealized analog of the subtropical ocean gyres with latent jets. In a broad agreement with Rypina et al. (2012), the diffusivity tensor was found to be anisotropic with the area-averaged value of $K_x/K_y \approx 5.2$. The evolution of three tracer patches – one in the subtropical gyre, one in the subpolar gyre, and one centered at the inter-gyre boundary – was examined in a full flow (“control run”) and a number of sensitivity runs with modified advection. The difference between sensitivity simulations was quantified using the weighted r.m.s difference with the control run (C_e).

Distribution of the tracer along the mean streamlines is very different between a control run and a simulation with the mean flow only (“no eddies”), which confirms the importance of the eddy-induced transport in the along mean-flow direction (Fig.28.5). If the anisotropic eddy diffusivity tensor is used in place of eddies in the “no eddies” simulations, the resulting distribution of tracer patches closely resemble the full flow. However, when an isotropic (but spatially inhomogeneous) diffusivity is used in place of the anisotropic tensor, C_e in the top layer increases from 0.41 (0.18) to 0.9 (0.53) in the subtropical (subpolar) gyres. This demonstrates that parameterized eddies will cause significant biases in tracer distribution if anisotropy in the eddy diffusivity is ignored.

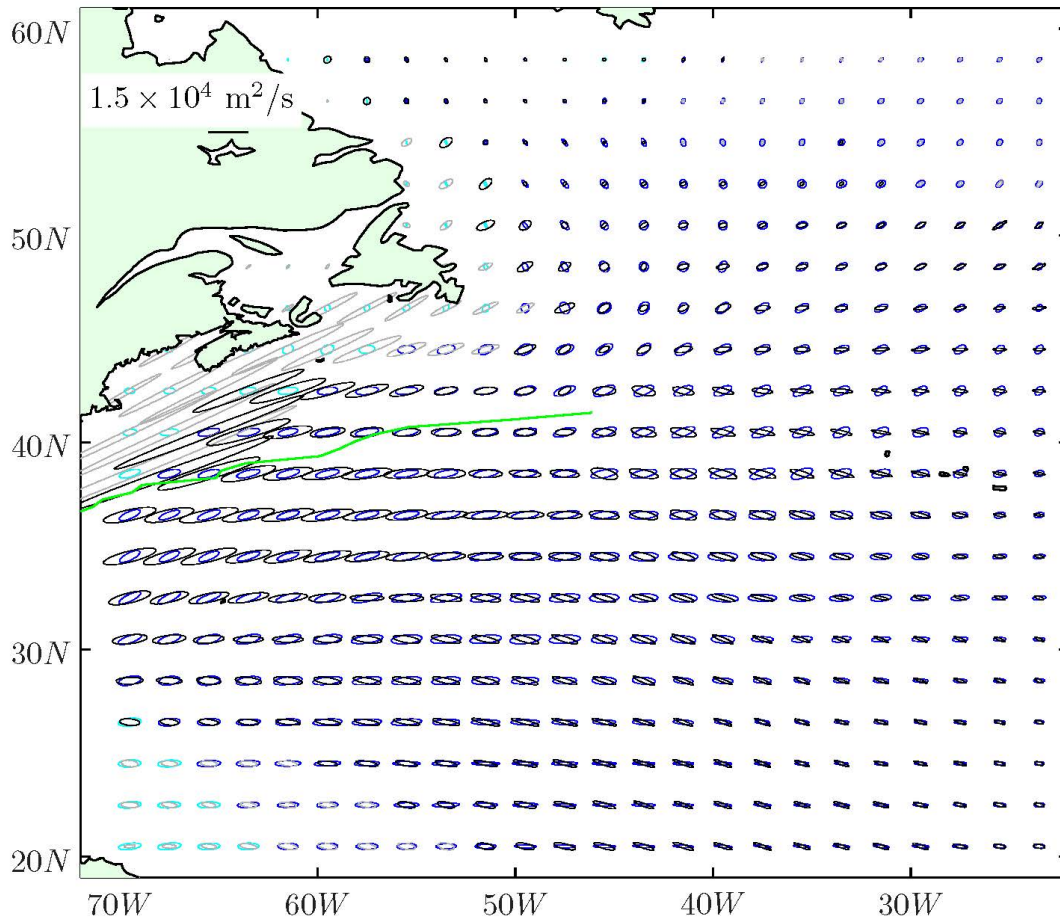


Figure 28.4 Evidence for inhomogeneous and anisotropic eddy transport. Eddy diffusivity computed from altimetric velocities: (1) eddy dispersion modulated by the mean flow (FTF method; black ellipses); (2) no effects of the mean flow (blue ellipses). Note that the transport remains strongly anisotropic even if the mean flow effects are removed. Gray and cyan ellipses show particle groups affected by the solid boundaries. Adapted from (Rypina et al., 2012). ©American Meteorological Society. Used with permission.

28.5 Transport in the presence of stationary jets

Strong observation- and model-based evidence for the transport anisotropy and its significance for tracer distribution calls for understanding of the underlying mechanisms. The Eulerian velocity variance cannot be used to explain the eddy-induced transport anisotropy, since the variance in the zonal and meridional velocities tend to be similar (Rypina et al., 2012). The answer must lie in the structure of the eddying flow and jets. Unlike molecular diffusion, caused by random motion of molecules, the eddy-induced material transport is driven by eddies that have well-defined length-scales and propagation velocity, and are embedded in the mean flow with jets. In this section, we discuss the following factors in the flows composed of eddies and stationary jets: eddy propagation relative to the mean current (section 28.5.1); transport barriers (sections 28.5.2 and 28.5.3); and shear dispersion on the jets (section 28.5.4).

28.5.1 Eddy propagation

The propagation of eddies relative to the mean jet flow can strongly influence the eddy-induced transport. For example, in

the case of eddies that propagate much faster than the typical speed of particle dispersion and do not trap particles, particles sample many different eddies that rapidly follow each other; therefore, τ_{corr} is short and the diffusivity is low. In contrast, a system with slowly propagating eddies can be very efficient in dispersing tracer particles, since the particles will spend a long time in each eddy and τ_{corr} is long. Observation-based estimates confirm that slowly propagating atmospheric eddies can be very efficient in inducing material transport (e.g. Randel and Held, 1991; d'Ovidio et al., 2009). In the limit of eddies standing relative to the mean flow, at the so-called steering or critical layers, the diffusivity can reach maximum values. In an analytical study of the transport properties of linear unstable waves in a broad mean atmospheric flow, Green (1970) derived an inverse relationship between the cross-stream diffusivity and the wave speed relative to the mean flow, and demonstrated the enhancement of diffusivity near the steering levels. Killworth (1997) proposed a parameterization of the eddy-induced property fluxes in the oceans; the resulting diffusivity is inversely proportional to the square of wave speed relative to the mean current and is a strong function of depth. The mid-depth max-

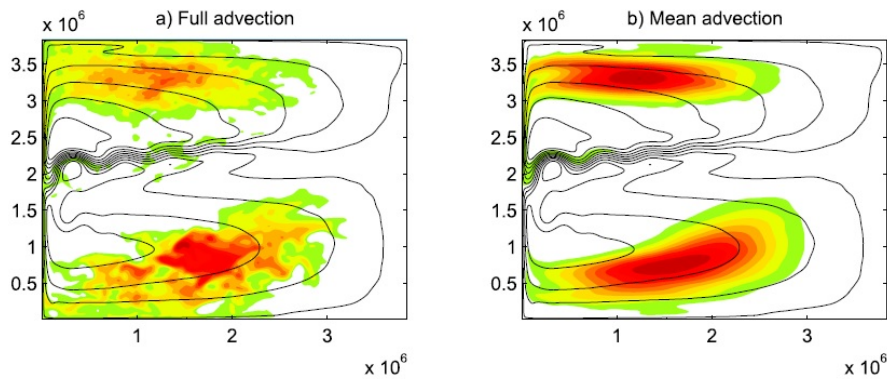


Figure 28.5 Color dye tracer concentrations in a QG double-gyre flow, day 100. a) Control simulation (full flow); b) Mean advection only (no eddies). Adapted from Kamenkovich et al. (2015). ©American Meteorological Society. Used with permission.

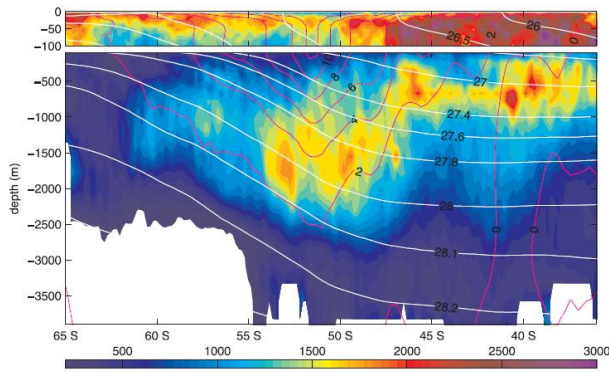


Figure 28.6 Isopycnal effective cross-stream diffusivity in the ACC (in $m^2 sec^{-1}$), calculated from passive tracer distribution and using velocities and densities from the 3D Southern Ocean State Estimate (SOSE). The magenta contour lines show the streamwise-averaged zonal velocity (mean ACC), and mean isopycnals appear in white. Note that the maximum diffusivity follows a particular velocity contour, shown to correspond to a steering level. Adapted from Abernathey et al. (2010b). ©American Meteorological Society. Used with permission.

imum of eddy diffusivity in the ACC, simulated in the Southern Ocean state estimate, is consistent with the enhancement of mixing at the steering levels (Fig.28.6; Abernathey et al., 2010b).

Further developing ideas from the linear studies, Ferrari and Nikurashin (2010b) considered the effects of propagating eddies in the presence of a horizontally uniform zonal background current U . The nonlinear dynamics is approximated by a linear system forced by a fluctuation-dissipation stochastic model, which excites waves with zonal wavenumber k , zonal phase speed c , and decorrelation timescale T . The meridional eddy diffusivity can then be derived analytically:

$$K_y = \frac{K_0}{1 + T^2 k^2 (c - U)^2}, \quad (28.4)$$

where K_0 is the maximum value at the steering level ($c = U$). This equation illustrates an overall suppression of the cross-flow diffusivity by the eddy propagation relative to the

mean flow. For example, the eastward (westward) U will have a suppressing effect on the eddy-induced transport by westward- (eastward-) propagating eddies, whereas the effects of the same U for eastward- (westward-) propagating eddies are less straightforward and can enhance the mixing. Ferrari and Nikurashin (2010b) used (28.4) to demonstrate the suppressing effects of U and explain spatial variability in the ACC diffusivity, estimated from observations and model simulations. Abernathey and Marshall (2013) found significant effects of the mean advection on cross-stream diffusivity in most of the ocean, with generally suppression by the eastward flows and enhancement by the western flow (in the tropics).

The application of (28.4) to more realistic multichromatic eddies and to strongly sheared jets is, however, not straightforward. Klocker et al. (2012) estimated parameters in (28.4) by fitting the equation into a set of simulations with realistic eddy fields and mean flows, and was able to validate the formula. Using a similar approach, Klocker and Abernathey (2014) analysed diffusivities in a series of synthetic flows consisting of altimetry-based eddy velocity estimates in the Eastern Pacific and various values of a uniform zonal flow U , and estimated K_0 and eddy propagation speed c . Consequent analysis demonstrates that the diffusivity in the full flow is in a good agreement with (28.4). Chen et al. (2015d) derived a multi-wavenumber formulation, which allowed calculation of K_y from the spectra of Eulerian eddy velocity. The resulting relation provides a closer match to the model- and data-based estimates of cross-flow diffusivity than the original single-wave theory (28.4).

The underlying assumption of these theories is that the mean jet flow is broad and spatially uniform, which implies that the mean jet changes on length scales longer than the typical size of eddies. It is, however, possible that the above results can be useful beyond their form applicability, and Eden (2011) used an equivalent of (28.4) to model suppression of mixing at jet cores (see section 28.5.3). Nevertheless, it is still possible that additional effects, such as shear dispersion and transport barriers, can overcome the importance of the above effects of the mean flow, when the width of the mean jet is comparable to the eddy length. This may explain why the suppressing effects of U on K_y were not found to be significant by Rypina et al. (2012) in the North Atlantic (Fig.28.4). It is also possible that the nonlo-

cal nature of Lagrangian methods and the large bin sizes used in this study may complicate detection of the suppression of eddy diffusivities by the mean flow.

28.5.2 Material transport barriers in a jet

A transport barrier is typically located in a jet core and separates regions of enhanced stirring located near the jet flanks on either side of the jet. These barriers are often "partial", that is, the transport across them is not zero ("absolute barrier") but reaches a well-pronounced minimum. Useful insight into the mechanism by which the shearless core of a jet acts as a barrier for the cross-jet transport can be gained from dynamical systems theory (Samelson, 1992; Rogerson et al., 1999; Haller, 2001a,b, 2002; Wiggins, 2005; Samelson and Wiggins, 2006; Rypina et al., 2007b,a, 2009; Beron-Vera et al., 2010; Farazmand et al., 2014). In this approach, the ocean is described as a nonlinear dynamical system whose phase space is separated into regions with qualitatively different motion that can exchange properties. In the case of a jet, the regions of interest correspond to the meandering jet core, where, similar to the steady flow, the particle spreading is very weak, and the jet flanks with much more vigorous particle spreading. Using the dynamical systems methodology, the motion is regular near the jet core and "chaotic" on either side of a jet. This picture is qualitatively consistent with the suppression of cross-stream diffusivity at the jet core and enhancement at steering levels on either side of the jet.

Further progress can be made by assuming that the flow under consideration is two-dimensional, spatially-periodic in one direction (such as the stratospheric polar jet or ACC), and consists of a steady background flow plus a small time-dependent multi-frequency perturbation. In a steady flow, all trajectories lie on closed streamlines, and each of them serves as an absolute transport barrier. Since in a zonally-periodic jet flow, these regular streamlines are closed curves, one can define a zonal period and the corresponding frequency of motion for each trajectory. When a time-dependent perturbation is added to the steady background flow, trajectories are no longer constrained to follow mean streamlines, and chaotic motion can occur. Importantly, however, not all regular trajectories are destroyed by the perturbation; some survive and act as transport barriers in the perturbed system. This is consistent (under the above conditions) with the famous Kolmogorov-Arnold-Moser theorem (KAM theorem; Kolmogorov, 1954; Arnold, 1963; Russman, 1989).

Chaos is induced by the resonances between the flow perturbations and those trajectories of the background steady flow whose frequencies are rationally-related to that of the perturbation. One can define a resonance width as the width of the chaotic layer around the resonant trajectory. When two resonances overlap, all regular trajectories in between are destroyed, and a broad well-mixed chaotic "mixing zone" is formed. This principle is known as the resonance overlap criterion (Zaslavsky and Chirikov, 1972; Chirikov, 1979) and is often used to define the onset of a wide-spread chaos. For a system consisting of a zonally-periodic steady jet subject to a small time-periodic or quasi-periodic disturbance, an analytical expression for the resonance width can be derived (Rypina et al., 2007b), predicting

that a resonance width is generally narrower near the shearless jet core than at the jet flanks. This implies that regular trajectories (and transport barriers) are more likely to survive near the jet core. This argument applies to both eastward and westward moving jets, but in practice the dynamics of unstable eastward and westward jets are different, and the former generally possess more robust transport barriers than the latter. Note also that within this framework, strong stirring is generally expected near resonance levels where a trajectory period is equal to that of the perturbation. This condition is equivalent to the steering level condition ($c = U$), thus providing a link between these two viewpoints.

Although the assumptions evoked above about the smallness of the perturbation, multi-frequency, time dependence, spatial periodicity, and infinite time interval do not formally apply to realistic meandering jets with strong eddies, in practice, the predictions made using these theoretical results often hold even in realistic settings. For example, generalized Lagrangian jet cores, or parabolic Lagrangian Coherent Structures, can be rigorously defined even in finite-time flows (Farazmand et al., 2014). The interested reader is referred to a review by Haller (2015) for a discussion of challenges and limitations of the dynamical systems approach to studying transport barriers in realistic geophysical flows.

On the applied side, Rypina et al. (2011) considered simulated drifter trajectories in the near-surface North Atlantic, in which the velocity field is derived from the real drifter trajectories and satellite altimetry. The results demonstrate the existence of a strong and robust transport barrier near the Gulf Stream core (Fig.28.7); see also Samelson (1992) for a similar conclusion in the case of an idealized meandering jet. Rypina et al. (2013) observed a similar transport barrier in the western Pacific Ocean near the core of the Kuroshio Current in their studies of the spread of the Fukushima-derived radionuclides. These results suggest that it might be typical for many strong ocean currents to inhibit cross-jet mixing; see also Farazmand et al. (2014).

28.5.3 Transport barriers in multiple zonal jets

In the system of alternating zonal jets, generated by barotropic randomly forced β -plane turbulence, the cores of the narrow eastward jets correspond to sharp PV gradients, whereas the broad westward jets correspond to zones of nearly uniform PV (e.g. Dritschel and McIntyre, 2008c). The formation of this so-called "PV staircase" is assumed to be caused by material transport barriers at the cores of eastward jets and broad mixing zones ("surf zones") at the westward jets. Since positions and intensities of the barriers and mixing zones are controlled by the transport of PV, which is materially conserved quantity up to diabatic processes, they are sensitive to the flow kinematics (Haynes et al., 2007b). In particular, all components of the flow, eddies and mean currents, are essential for the existence of barriers.

Close connection between the meridional structure in PV and eddy diffusivity component K_y can be illustrated by the following argument. Consider first a barotropic QG flow with zonal jets and separate the PV denoted by q and velocities, (u, v) , into the zonal mean (denoted by the overbar) and eddies (denoted

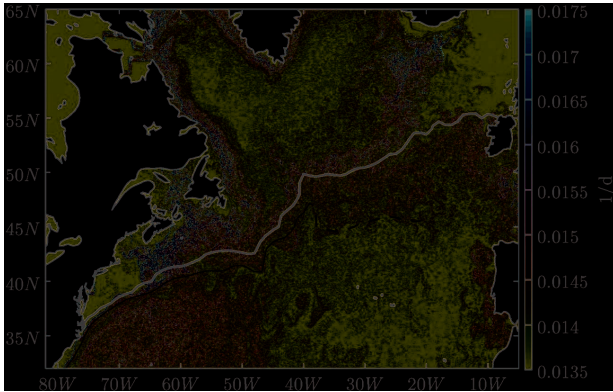


Figure 28.7 Forward-time Finite-Time Lyapunov Exponents (FTLEs) on 6 Jan 1993 with a 6-months integration time. Yellow/red colors indicate more chaotic regions, and blue colors indicate more regular regions. The white curve approximates the mean Gulf Stream core position. FTLE measures the maximum separation rate between a trajectory and its close neighbors, and regions with inhibited stirring (partial transport barriers) are characterized by low FTLEs. In particular, note the blue ribbon near the western portion of the Gulf Stream. Adapted from Rypina et al. (2011). ©American Meteorological Society. Used with permission.

by primes). The mean PV is $\bar{q} = \beta y - \frac{d\bar{u}}{dy}$, where β is planetary vorticity gradient; \bar{q} is taken to be time-independent. The PV balance can be written as

$$\frac{\partial q'}{\partial t} + \frac{\partial}{\partial x} uq' + \frac{\partial}{\partial y} v'q' = \kappa \nabla^2 \left(\frac{\partial v'}{\partial x} - \frac{\partial u'}{\partial y} - \frac{d\bar{u}}{dy} \right) \quad (28.5)$$

where κ is Laplacian viscosity. Forcing (PV source) can be easily included in this derivation but is neglected here for the sake of transparency. Taking the zonal mean and assuming that the meridional eddy PV flux $\overline{v'q'}$ can be approximated by the down-gradient diffusion, we can write

$$\frac{d}{dy} (K_y(y) + \kappa) \frac{d\bar{q}}{dy} = 0, \quad (28.6)$$

from which we can easily find K_y :

$$K_y(y) = \frac{C_0}{\beta - \frac{d^2\bar{u}}{dy^2}} - \kappa, \quad (28.7)$$

where C_0 is a constant. For positive K_y , C_0 has to be sufficiently large, and the gradient of PV cannot change sign, that is, the mean zonal flow is barotropically stable. Upgradient PV fluxes (negative K_y), however, cannot be excluded. The above expression demonstrates that K_y has maxima (a "surf zone") where $\frac{d^2\bar{u}}{dy^2}$ has positive maxima, that is, at the cores of westward jets, and minima (a barrier), where $\frac{d^2\bar{u}}{dy^2}$ has negative minima, that is, at the cores of eastward jets.

For a two-layer baroclinic flow, the mean meridional PV gradient in the n^{th} layer is

$$\frac{dq_n}{dy} = \beta - \frac{d^2\bar{u}_n}{dy^2} + (-1)^{n+1} \frac{f^2}{g'H_n} (\bar{u}_1 - \bar{u}_2), \quad (28.8)$$

where H_n is the layer thickness, f – the Coriolis parameter, g' – the reduced gravity and $n = 1, 2$. By following the same steps as in the barotropic case, an analog to (28.7) can be derived:

$$K_y(y) = \frac{C_0 + \kappa \frac{d^2\bar{u}_n}{dy^2}}{\beta - \frac{d^2\bar{u}_n}{dy^2} + (-1)^{n+1} \frac{f^2}{g'H_n} (\bar{u}_1 - \bar{u}_2)}, \quad (28.9)$$

From (28.9) it is clear that the position of maxima and minima in K_y can be different between the two layers.

Berloff et al. (2009d) focused on baroclinic flows with multiple, alternating zonal jets and found that such flows can be characterized by different sets of partial barriers and mixing zones aligned with the jets. First, PV profiles do not closely approach the "ideal PV staircase". Although the meridional distribution of the PV is inhomogeneous, only a modest (less than a factor of 2) enhancements of the PV gradient relative to the background value exists. Second, Berloff et al. (2009d) found that the patterns of partial barriers and mixing zones are significantly more complex than in the single-layer models described above. The simplest measure of the material transport can be obtained by counting particles that crossed a particular latitude; the total meridional material flux, $M_{tot}(y)$ was found by dividing the total number of particles in the corresponding ensemble by the time interval. A substantial part of $M_{tot}(y)$, however, corresponds to the particles that oscillate back and forth in the meridional direction, and, thus, do not participate in irreversible meridional transport. The irreversible component $M_{irrev}(y)$ of the total transport is obtained by conditional counting of only those particles that changed their PV.

The total and irreversible meridional fluxes have complicated pattern in relation to the underlying jets (Fig. 28.8), and $M_{irrev}(y)$ is generally a much more accurate detector of the barriers and mixing zones. Overall, the irreversible transport constitutes between the quarter and half of the total transport, depending on the flow regime and isopycnal layer depth. The pronounced partial barriers correspond to the eastward jet cores only for the flow regime driven by the eastward background shear and only for the upper isopycnal layer. In this flow regime, the deep isopycnal layer cores of the eastward jets are not barriers but, on the opposite, intense mixing zones. In the flow regime driven by westward background shear, contrast between the partial barriers and mixing zones is relatively weak; in the upper layer the barriers are located between the eastward and westward (relative to the background flow) jets, and in the lower layer the barriers are located on the southern flanks of the westward jets. Note that although $M_{tot}(y)$ and $M_{irrev}(y)$ are useful for identifying transport barriers, the relationship of both of these Lagrangian diagnostics to the Eulerian diffusivity K_y is not straightforward.

The dynamical systems-based arguments (section 28.5.2) do not, however, make a distinction between eastward and westward jets and predict the existence of shearless-type transport barriers at the cores of both eastward and westward jets. These predictions are in fact supported by the fact that most boundaries between zones and belts in the Jovian atmosphere correspond to prograde and retrograde jets and by the suppression of mixing at the core of the westward subtropical jet in the Earth stratosphere (see 28.3; Beron-Vera et al., 2008a). Beron-Vera et al. (2008a) presented evidence for the existence of transport barriers at the cores of both eastward and westward jets by

analysing particle trajectories in an equivalent-barotropic QG system initialized with an idealized PV staircase and random-phase perturbations. The results indicated the absence of material exchange and very low values of FTLEs across both eastward and westward jets, as would be typical for meridional transport barriers. Mixing zones associated with vigorous water mass exchange and large FTLE values were observed at jet flanks between the jet cores. The barriers on westward and eastward jets were nevertheless different. Notably, the barriers at the westward jets were broader and less robust with respect to the magnitude of the imposed PV disturbance, and they were easier destroyed by large perturbations than the barriers on the eastward jets.

These results can potentially be used to interpret the absence of barriers on westward jets in the studies described in the rest of this section, in which the eddy field is in a statistical equilibrium with the jets. Chapter 29 further reports the absence of complete transport barriers in forced barotropic turbulent flows with jets, and tracer distribution in their studies shows signs of only weak partial barriers if the forcing is present. Further research in more realistic flows is needed to understand when and why barriers on jet cores can be broken by eddies and small-scale currents, and characterization of turbulent flows in terms of the flow regimes and energy cascade would be required for reconciliations of results discussed in this section.

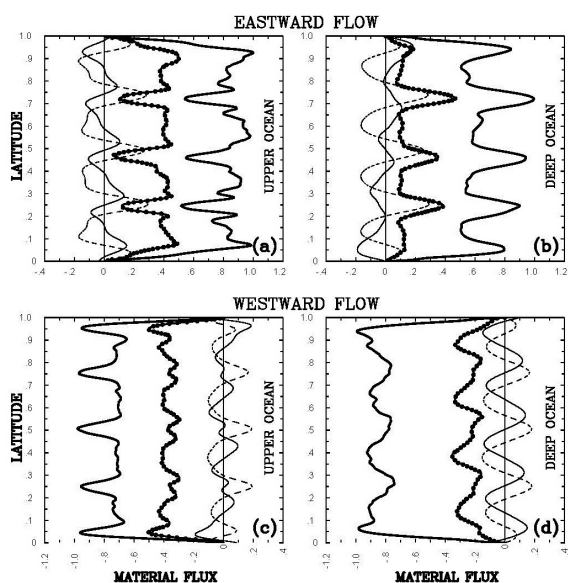


Figure 28.8 Meridional material transport in the eddy baroclinic flow characterized by multiple alternating jets. Considered are flow regimes maintained by eastward (upper panels) and westward (lower panels) background shears; the transport properties are shown for upper-ocean (left panels) and deep-ocean (right panels) isopycnal layers. Total, $M_{tot}(y)$, and irreversible, $M_{irrev}(y)$, material fluxes are shown with the thick line and thick line with dots, respectively. The corresponding profiles of the isopycnal PV anomaly and zonal velocity of the time-mean jets are shown aside with thin and dashed lines, respectively. Adapted from Berloff et al. (2009d). ©American Meteorological Society. Used with permission.

28.5.4 Shear dispersion in stationary jets

In shear dispersion, the stirring of a tracer across the sheared current leads to suppressed along-current dispersion of the tracer. In the case of a sheared zonal jet, this can be interpreted as a result of reduction in the zonal decorrelation scales due to eddy stirring in the transverse direction.

In a seminal paper, Taylor (1953) considered dispersion of a tracer along a pipe and derived a simplified equation for the tracer evolution, widely used in many applications of fluid dynamics (e.g., Young et al., 1982; Young and Jones, 1991). Smith (2005a) applied these ideas to tracer distribution in the flow consisting of isotropic eddies and multiple alternating zonal jets. He assumed that the eddy-induced transport in the meridional direction is purely diffusive with constant diffusivity K_y . An analytical relationship between K_x and K_y then takes the following form:

$$K_x = \frac{1}{K_y} \sum_{n=-\infty}^{\infty} \frac{|\hat{U}_n|^2}{l_n^2} \quad (28.10)$$

where U_n and l_n is the n^{th} Fourier coefficient and the corresponding meridional wavenumber for $U(y)$:

$$U(y) = \sum_{n=-\infty}^{\infty} \hat{U}_n e^{-il_n y} \quad (28.11)$$

Numerical simulations in this study confirmed the validity of (28.10) and demonstrated that as β is reduced and zonal jets are weakened, K_y increases and K_x decreases, leading to more isotropic mixing. This dependence on β is consistent with earlier studies (Holloway and Kristmannsson, 1984; Bartello and Holloway, 1991). Note, however, that K_x in (28.10) describes a joint effect of the mean jets and eddies, and is not, formally speaking, an eddy-induced diffusivity. The distinction can be particularly important if K_x is used to parameterize eddies in coarse-resolution numerical models that can only simulate the mean currents. Eddy-induced diffusivity must be used in these situations in order to avoid erroneous non-diffusive behavior (section 28.7.1) and “double-counting” the dispersion by the mean flow.

The inverse relationship between K_x and K_y implies that reduced meridional mixing corresponds to enhanced zonal material transport. This reduction can take place for several reasons. As we have seen in the previous section, material transport barriers in zonal jets and mixing suppression by the mean flow will each act to reduce K_y . More generally, a meridional Lagrangian l_{corr} for tracer particle in a zonal flow with a strong shear is likely to be short, because the shear will tear the particles away from each particular eddy. These effects will reduce K_y and enhance K_x , increasing the anisotropy of the transport.

28.6 Anisotropic eddies and transient jets

Studies of the role of the mean jets described in the previous sections rely on the assumption of scale separation between

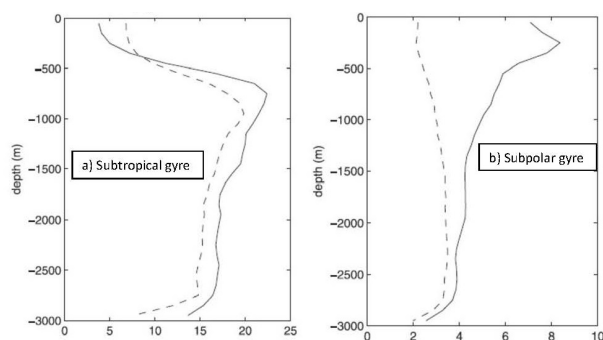


Figure 28.9 The ratio K_x/K_y with diffusivities estimated from simulated Lagrangian trajectories in a numerical model of the North Atlantic, as a function of depth. The left panel shows the estimates from the subtropical gyre interior; the right panel – the subpolar gyre. The solid lines show the control simulation, the dashed lines – the eddy-only sensitivity run (no jets). Adapted from Kamenkovich et al. (2009a). ©American Meteorological Society. Used with permission.

the mean currents with jets and the eddy field. These assumptions are valid for atmospheric flows, and such energetic mean oceanic currents as the Gulf Stream and ACC. However, significant anisotropy in the eddy-induced material transport was found in the presence of weak mean flows and relatively strong eddies. In particular, Rypina et al. (2012) showed that the diffusivities are anisotropic in the interior of the North Atlantic subtropical gyre and that the effects of mean advection on this anisotropy are weak (Fig.28.4). Stationary alternating zonal jets in the oceans tend to be latent (Berloff et al., 2009d; Kamenkovich et al., 2009e; Berloff et al., 2011b), and their direct contribution to the material transport can, therefore, be expected to be small.

Kamenkovich et al. (2009e), in a numerical study of the North Atlantic circulation, found latent stationary jets in the southern part of the domain (subtropical gyre) and more powerful jets in the northern part (subpolar gyre). Kamenkovich et al. (2009a) used (28.2) and estimated eddy diffusivities with the degree of anisotropy K_x/K_y exceeding 20 at intermediate depth in the subtropical gyre (solid lines in Fig.28.9a). The relative importance of jets and eddies was then analysed in a sensitivity run, in which Lagrangian particles are advected by the eddy flow only, with the time-mean jets removed. The FTF method was not used, and the jets had no effect on particle dispersion. The removal of jet advection did not, however, lead to significant changes in the anisotropic material transport (dashed lines in Fig.28.9a) in the subtropical gyre. This result demonstrates that the anisotropy is due to transient eddies, rather than the stationary jets. In contrast, the removal of the jets in the subpolar region, where they are more powerful, leads to more isotropic diffusivities (Fig.28.9b); K_x/K_y is, however, still larger than 2.

How can eddies induce anisotropic transport even in the absence of time-mean advection? The explanation must involve anisotropic properties of the eddy flow, such as predominantly zonal propagation (already discussed in section 28.5.1) or the anisotropic structure of the eddies themselves.

We remind the reader that eddies are defined here as all deviations from the mean flow, and this definition includes, for

example, non-stationary (propagating) jets. For example, zonal jets were shown to drift in the meridional direction in midlatitude ocean gyres (Richards et al., 2006c; Kamenkovich et al., 2009e; Chen et al., 2016a) and in idealized flows in which the mean PV gradient is not meridional (section 28.7.2, Boland et al., 2012b). Propagating zonally- and meridionally-elongated patterns were observed in altimetry-based estimates of near-surface velocity anomalies (Huang et al., 2007b). Kamenkovich et al. (2015) examined a two-dimensional, wavenumber ($k-l$) spectrum (Fig.28.10) of the time-dependent component of the double-gyre flow and altimetry-derived circulation of the North Atlantic. They discussed an anisotropic peak at long zonal and finite meridional scales ($k \ll l$) and referred to the corresponding “jet-like” component of the flow as Zonally-Elongated Large-Scale Transients (ZELTs). Despite corresponding to only a modest portion of the total energy ($\sim 15\%$ in the top layer), ZELTs are very efficient at stirring properties in the zonal direction. The latter property can be understood as a predominantly zonal Stokes drift; see an analytical example in Kamenkovich et al. (2009a).

ZELTs’s presence in the flow explains a large portion of transport anisotropy, as was demonstrated by simulations of Lagrangian particles in a QG double-gyre flow (Kamenkovich et al., 2015). Diagnosed diffusivity tensor in the full flow is strongly anisotropic, which is explained by zonal l_{corr} being longer than the meridional ones, since the velocity variance is similar in both directions (see also Rypina et al., 2012). Filtering out ZELTs (that is, removing zonal scales longer than 30 Rossby deformation radii) led to dramatic reduction in the anisotropy coefficient K_x/K_y from 5.2 (area-averaged) to 2.0. A similar reduction (from 5.4 to 2.5) was observed in an analogous set of Lagrangian simulations with altimetric velocities. The remaining anisotropy is most likely caused by the mean currents, since the FTF method employed in this study accounts for the modulation of K_x and K_y by the mean flow (sections 28.5.1 - 28.5.3).

The exact mechanism by which ZELTs can cause the eddy-induced transport to be anisotropic remains to be established. Analysis of synthetic channel flows (Kamenkovich et al., 2017, to be submitted), suggest that ZELTs act to produce a predominantly zonal material transport, but eddies with short zonal lengthscales act to disperse particles meridionally and to reduce the zonal dispersion. The resulting inverse relationship between the zonal and meridional dispersion is analogous to Equation 28.10, and the anisotropy can thus be interpreted as a shear dispersion on transient ZELTs.

28.7 Importance of other factors

28.7.1 Non-diffusive behavior

In a purely diffusive process, the eddy-induced dispersion of Lagrangian particles grows linearly in time (section 28.2), but in realistic oceanic and atmospheric flows with jets it can be faster or slower than linear, that is “superdiffusive” or “subdiffusive”, respectively. Superdiffusive spreading can be caused by, for example, the presence of a persistent velocity shear in a jet. In the extreme example of a flow composed entirely of steady zonal

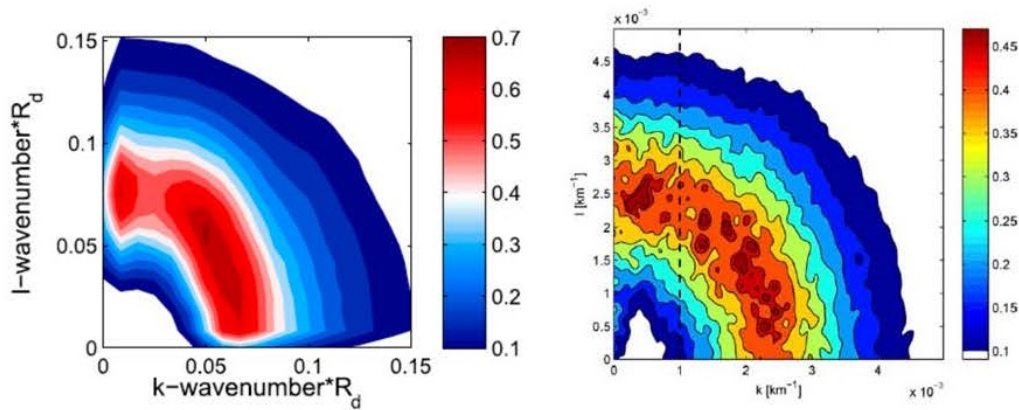


Figure 28.10 Wavenumber $k-l$ spectra of velocity in the North Atlantic. Left panel: top layer of the baroclinic QG double-gyre flow; the spectrum is averaged over 50 years and non-dimensionalized by the total kinetic energy, wavenumbers are non-dimensionalized by the first Rossby deformation radius. Right panel: inferred from the AVISO satellite altimetry, time averaged over the period from 1992 to 2009; units are $\text{km}^2 \text{day}^{-2}$. Adapted from Kamenkovich et al. (2015). ©American Meteorological Society. Used with permission.

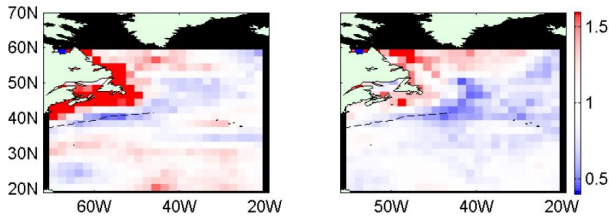


Figure 28.11 Non-diffusive spreading of Lagrangian particles in the North Atlantic. These effects are quantified using a parameter α that describes a power-law behavior of the dispersion in time: $\alpha = 1$ implies purely diffusive spreading, $\alpha < 1$ subdiffusive, and $\alpha > 1$ superdiffusive behavior. Left panel describes the spreading in the direction of maximum transport, right panel the direction of minimal transport. Adapted from Rypina et al. (2012). ©American Meteorological Society. Used with permission.

jets, the particle dispersion will grow quadratically with time, in the so-called ballistic regime. To see this, consider a group of particles with initial positions $(x_n(0), y_n(0))$ and assume a meridional velocity shear $\bar{u}(y)$ that advects them. The dispersion in the x -direction is then given by (y_n do not change with time):

$$D = \frac{t^2}{N} \sum_{n=1}^N \left(\bar{u}(y_n) - 1/N \sum_{n=1}^N \bar{u}(y_n) \right)^2. \quad (28.12)$$

Transient eddy activity will cause the dispersion to deviate from the purely ballistic spreading, but the dispersion will remain superdiffusive if the l_{corr} are long. In particular, our experience shows that zonal particle dispersion remains superdiffusive in a flow with strong multiple jets, unless dispersion by the jets is corrected for (as in the FTF method). Note that these non-diffusive effects cannot be captured by methods that are based on the diffusive model, such as the tracer contour-based method of Nakamura (1996b), which can lead to serious biases in diffusivity estimates. Spatial inhomogeneity of the eddy field can also cause non-diffusive particle dispersion, if

the Lagrangian particles enter regions with substantially different eddy fields. Alternative non-diffusive transport models have been proposed in the past (e.g., Berloff and McWilliams, 2003), but their practical implementations are limited so far.

Rypina et al. (2012) demonstrated that parts of the North Atlantic basin exhibit super- or subdiffusive spreading both in the directions of the maximum and minimal spreading (Fig. 28.11). In particular, tracer particles leaving the Gulf Stream encounter a weaker eddy field, which slows their spreading in the cross-stream direction and leads to subdiffusive behavior. The deviations from the diffusive regime also depend on the particular direction, further contributing to the anisotropy of the material transport.

28.7.2 Topography and the mean PV distribution in the oceans

Zonally-varying topography and nonzonal large-scale circulation cause deviations of the mean potential vorticity (PV) gradient from the meridional direction, which can introduce a wealth of additional effects on the direction and magnitude of the anisotropic eddy-induced transport. Enhanced eddy stirring near topographic features was reported by several studies (Griesel et al., 2010; Thompson, 2010b). In particular, Thompson and Sallee (2012) used altimetry-based velocities to demonstrate enhancement of cross-frontal mixing downstream of topographic ridges; their idealized simulations demonstrate reorganization of zonal jets downstream of zonal ridges, leading to the weakening of meridional transport barriers; see also Section 2.5.3 in this book. The eddy variability can be expected to be larger in the lee of meridional topographic ridges, due to enhancing effects of zonal topographic slopes on baroclinic instability (Chen and Kamenkovich, 2013). Boland et al. (2012b) further showed that large-scale zonal topographic slopes lead to non-zonal and meridionally migrating multiple jets; similar effects were observed downstream of meridional ridges (Chen et al., 2015b). Enhanced eddy energy over the zonal slope, in comparison to the flat-bottom case, results in the weakening of

the transport barriers at the jet cores, but anisotropy in the eddy-induced transport remains significant.

LaCasce and Speer (1999) found that the eddy-induced particle dispersion in idealized barotropic flows is mostly along contours of f/H , with water depth H and Coriolis parameter f , which are the contours of mean PV in this case. They also reported considerable f/H control on the observed floats, and the difference between dispersion along and across f/H contours was found greater than the difference between zonal and meridional dispersion (LaCasce and Bower, 2000a). Similarly, O'Dwyer et al. (2000) demonstrated enhanced dispersion of floats in the direction parallel to the contours of the time-mean PV (fig.28.3). The situation becomes more complicated in flows where the PV contours are nonzonal and change their orientation with depth, due to the mean velocity shear and topography. For example, the analysis of Rypina et al. (2012) demonstrated that the direction of maximum diffusivity is generally not parallel to either the PV or f/H contours in their study.

28.8 Summary and implications for studies of tracer distribution

The studies summarized in this chapter demonstrate that the material eddy-induced transport depends on direction and geographical location, and that this anisotropy can be partly explained by the effects of mean advection and elongated (“jet-like”) transient flows. In particular, multiple zonal jets can alter the propagation of eddies, cause shear dispersion and non-diffusive particle spreading, and exhibit meridionally inhomogeneous transport properties that are often associated with transport barriers. All these effects frequently act to enhance the along-jet and suppress the cross-jet material transport, and are significant even if the jets are latent (i.e. their magnitudes are weaker than those of eddies). The transient eddy field is also anisotropic and it includes zonally-elongated patterns (ZELTs), which can explain a large part of the transport anisotropy, especially in oceanic flow regimes characterized by the latent jets.

The mechanisms of property transport discussed in this chapter suggest that anisotropic transport is governed by propagating transient patterns and their interactions with the jets. These effects can explain significant deviations from isotropic turbulent diffusion traditionally used to describe and parameterize the eddy-induced mixing of various properties. In particular, these non-local mechanisms can render parameterization of the eddy transport based on local properties nearly impossible. Understanding of the mechanisms for anisotropic transport, however, remains inadequate, and is primarily derived from highly idealized analytical and numerical models. The questions that need to be addressed in future idealized and realistic settings are:

(i) What mechanisms determine the dominant direction and magnitude of the anisotropic transport? This question is particularly intriguing if the mean PV gradients are non-meridional and depth-dependent.

(ii) How does propagation of various transient patterns influence the material transport? In particular, propagation of eddies relative to the mean zonal current was shown to suppress the transport, but this suppression has not been studied in the case of horizontally sheared, two-dimensional currents.

(iii) What are the implications of interactions between various components of the flow? For example, ZELTs play an important role in the zonal transport and its anisotropy, but their origins and the mechanisms of their interactions with the rest of the flow remain unclear.

(iv) What mechanisms lead to the formation of partial or complete transport barriers and enhanced mixing zones, and what processes determine their efficiencies? Detection and explanation of meandering transport barriers is particularly relevant to realistic geophysical and planetary flows.

(v) What is the relationship between instantaneous Lagrangian transport characteristics (i.e. FTLE ridges or Lagrangian coherent structures) and mean transport metrics such as particle dispersion and Eulerian diffusivity? The latter quantity is widely used to parameterize eddies in numerical simulations, and the applicability of Lagrangian estimates remains to be established.

(vi) What are the mechanisms and implications of non-diffusive transport? The eddy-induced transport can be expected to be non-diffusive in many parts of the oceans, which can increase anisotropy of the transport and limit the applicability of the diffusion model.

(vii) What is the importance of coherent vortices? These vortices can trap material inside their cores and carry it over significant distances, and, therefore, contribute to the anisotropy.

(viii) What is the role of topography, lateral boundaries and non-geostrophic motions? In particular, this chapter addresses only geostrophic eddies, whereas non-geostrophic motions can affect the eddy-induced transports through strong horizontal and vertical advection.

The importance of transport anisotropy for tracer distribution has long been recognized, and there is also sufficient evidence for the importance of jets. For example, failure to account for the difference between enhanced along-jet and suppressed cross-jet transports can obviously lead to erroneous eddy transport. On the other hand, substantial biases in the simulated tracer distribution can result if the along-jet eddy transport is neglected in a numerical model, especially in flows where the mean currents are less energetic than the eddy field. Finally, implications of non-diffusive spreading remain poorly understood, but may prove to be important. All these biases can negatively impact climate predictions. It is, therefore, important to recognize the need to depart from the commonly used eddy parameterizations based on isotropic and spatially homogeneous eddy diffusion. The complexity of the anisotropic transport also raises an important question: Is full resolution of oceanic eddies the only way to accurately account for the eddy-induced transport in ocean components of climate models? A positive answer may seem straightforward, but is not going to be a practical option for years to come, which increases the practical relevance of studies of the anisotropic eddy-induced transport.